Cancer Cell, Volume *27*

Supplemental Information

Acetyl-CoA Synthetase 2 Promotes Acetate Utilization and Maintains Cancer Cell Growth under Metabolic Stress

Zachary T. Schug, Barrie Peck, Dylan T. Jones, Qifeng Zhang, Shaun Grosskurth, Israt S. Alam, Louise M. Goodwin, Elizabeth Smethurst, Susan Mason, Karen Blyth, Lynn McGarry, Daniel James, Emma Shanks, Gabriela Kalna, Rebecca E. Saunders, Ming Jiang, Michael Howell, Francois Lassailly, May Zaw Thin, Bradley Spencer-Dene, Gordon Stamp, Niels J.F. van den Broek, Gillian Mackay, Vinay Bulusu, Jurre J. Kamphorst, Saverio Tardito, David Strachan, Adrian L. Harris, Eric O. Aboagye, Susan E. Critchlow, Michael J.O. Wakelam, Almut Schulze, and Eyal Gottlieb

SUPPLEMENTAL DATA

A

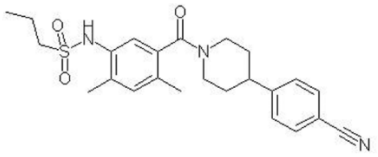

B

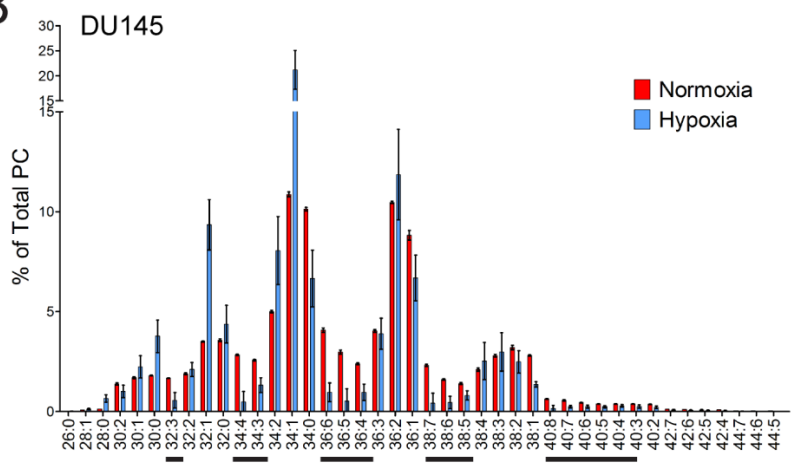

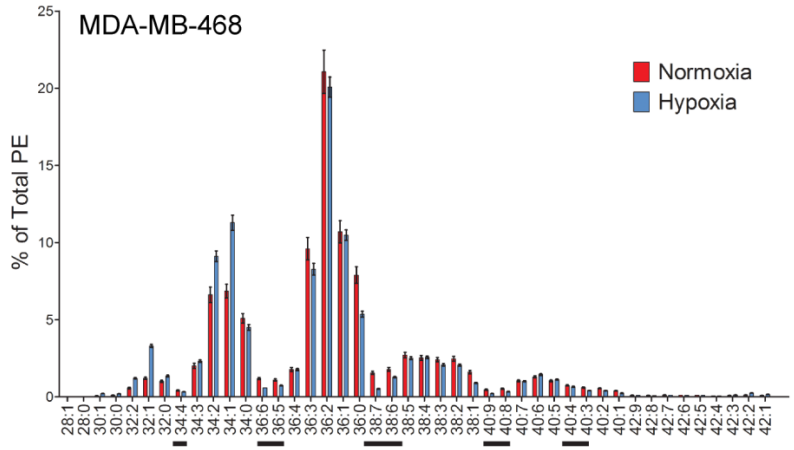

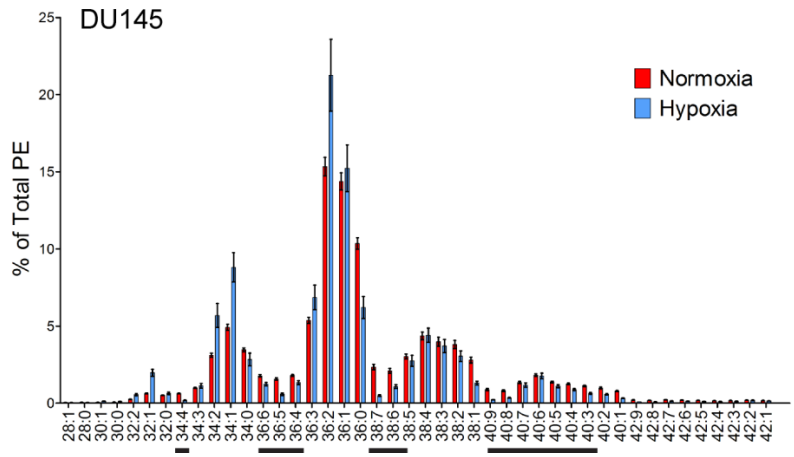

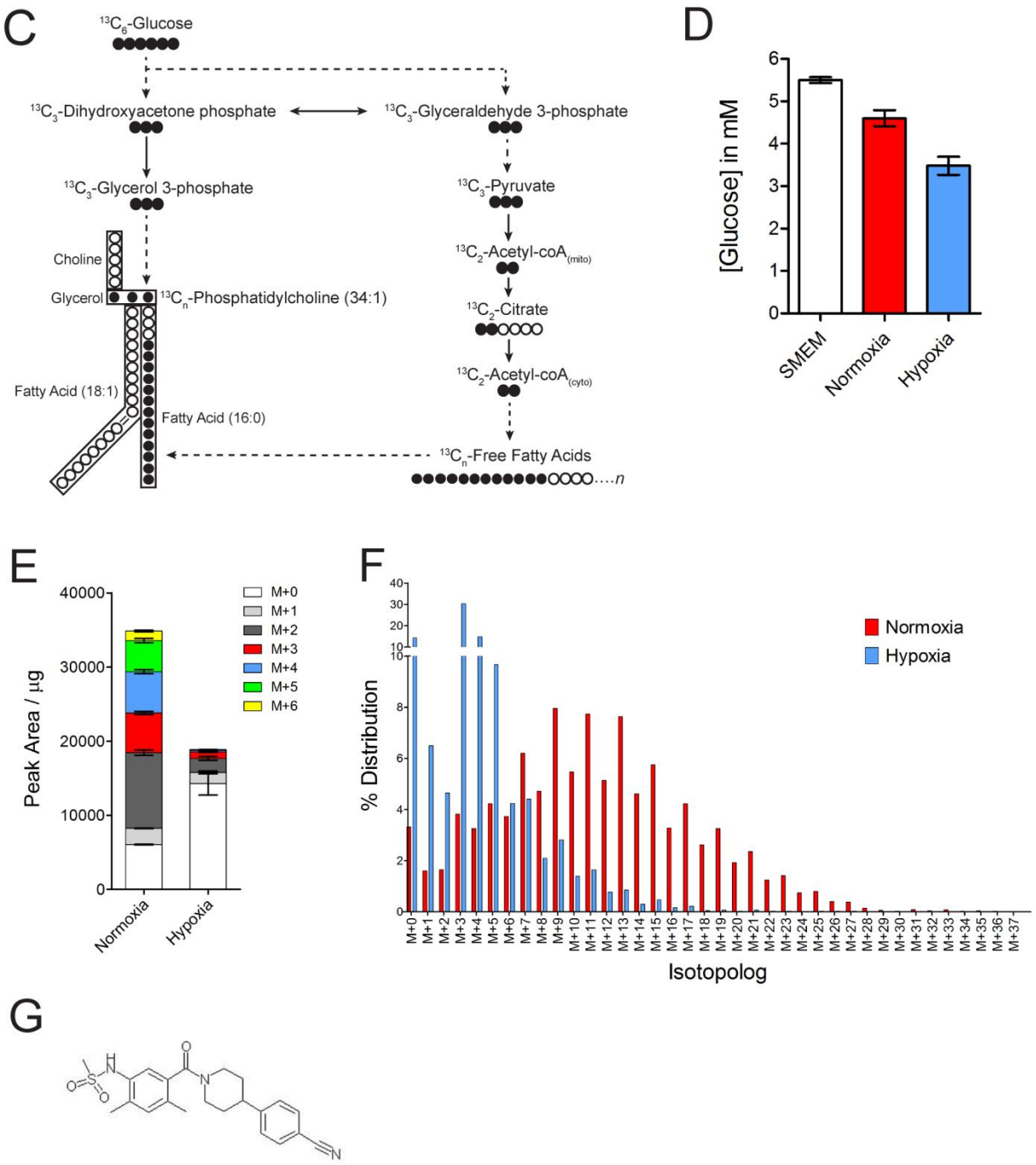
C
$^{13}C_6$-Glucose
$^{13}C_3$-Dihydroxyacetone phosphate
$^{13}C_3$-Glyceraldehyde 3-phosphate
$^{13}C_3$-Glycerol 3-phosphate
$^{13}C_3$-Pyruvate
Choline
$^{13}C_2$-Acetyl-coA$_{(mito)}$
Glycerol
$^{13}C_n$-Phosphatidylcholine (34:1)
$^{13}C_2$-Citrate
$^{13}C_2$-Acetyl-coA$_{(cyto)}$
Fatty Acid (18:1)
Fatty Acid (16:0)
$^{13}C_n$-Free Fatty Acids
....n
D
[Glucose] in mM
SMEM
Normoxia
Hypoxia
E
Peak Area / µg
M+0
M+1
M+2
M+3
M+4
M+5
M+6
Normoxia
Hypoxia
F
% Distribution
Normoxia
Hypoxia
Isotopolog
G

Figure S1, related to Figure 1. Hypoxia Induced a Shift to Shorter More Saturated Phospholipids. (**A**) Chemical structures of AZ22. AZ22 was identified in a high throughput screen of the AstraZeneca compound collection and a bis-amide hit was further optimized to improve FASN potency and absorption, distribution, metabolism and excretion (ADME) properties to deliver AZ22. This is exemplified in patent WO2008075070. (**B**) The lipid profile for PC and PE in MDA-MB-468 and DU145 cells cultured in SMEM + 1% serum at the indicated oxygen level was obtained by LC-MS/MS (See Table S1 for formulation of SMEM). PC and PE species containing highly polyunsaturated acyl chains (≥ 3 C=C bonds) are underlined. Data are presented as mean ± s.d. (n = 3). (**C**) Illustration depicting the flow of carbon from glucose to PC through two separate metabolic pathways. Glucose can contribute to phospholipid synthesis via provision of glycerol-3-phosphate or fatty acids. Dotted lines represent multiple steps, solid lines represent direct enzymatic reactions. (**D**) Glucose uptake in BT474c1 cells cultured SMEM + 1% serum at the indicated conditions. Data are presented as mean ± s.e.m. (n ≥ 3). (**E**) BT474c1 cells were incubated with SMEM + 1% serum containing 5.5 mM $^{13}C_6$-glucose for 24 hr in normoxia and hypoxia and the abundance of citrate isotopologs was quantified by LC-MS. Data are present as mean ± s.d (n = 3) (**F**) MDA-MB-468 were incubated with SMEM + 1% serum containing 5.5 mM $^{13}C_6$-glucose for 24 hr in normoxia and hypoxia and the abundance of PC(34:1) isotopologs was quantified by LC-MS/MS. Isotopologs represent the 24 hr labeling of PC(34:1) from $^{13}C_6$-glucose-derived fatty acids and glycerol 3-phosphate in MDA-MB-468 cells. 3 individual samples were pooled and run together. (**G**) Chemical structure of AZ62. See panel A for further details.

Table S1, related to Figure 1. Formulation of Serum-like Modified Eagles Medium (SMEM).

	SMEM		SMEM
Amino Acids	**µM**	**Vitamins**	**µM**
L-Alanine	510	Choline chloride	7.1
L-Arginine	64	D-Calcium pantothenate	2.1
L-Asparagine	41	Folic Acid	2.3
L-Aspartic acid	6	Niacinamide	8.2
L-Citrulline	55	Pyridoxine hydrochloride	4.9
L-Cystine	65	Riboflavin	0.3
L-Histidine	120	Thiamine hydrochloride	3
L-Glutamic acid	98	i-Inositol	11.1
L-Glutamine	650	**Inorganic Salts**	**µM**
L-Glycine	330	Calcium Chloride	1800
L-Isoleucine	140	Ferric Nitrate	
L-Leucine	170	Magnesium Sulfate	813
L-Lysine	220	Potassium Chloride	5330
L-Methionine	30	Sodium Bicarbonate	44050
L-Ornitine	80	Sodium Chloride	118706
L-Phenylalanine	68	Sodium Phosphate monobasic	1010
L-Proline	360	**Other Components**	**µM**
L-Serine	140	D-Glucose	5500
L-Threonine	240	Phenol Red	25
L-Tryptophan	78	Sodium Pyruvate	100
L-Tyrosine	74	Taurine	130
L-Valine	230		

The concentration of acetate in DMEM + 10% serum and SMEM + 10% serum ranged from 88-104 µM.

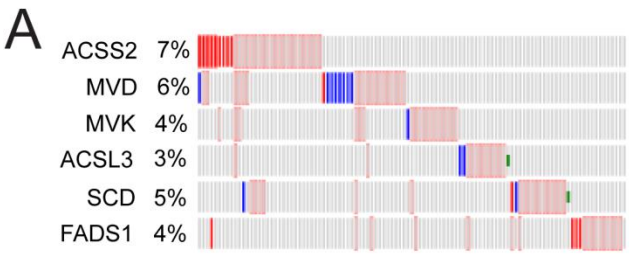

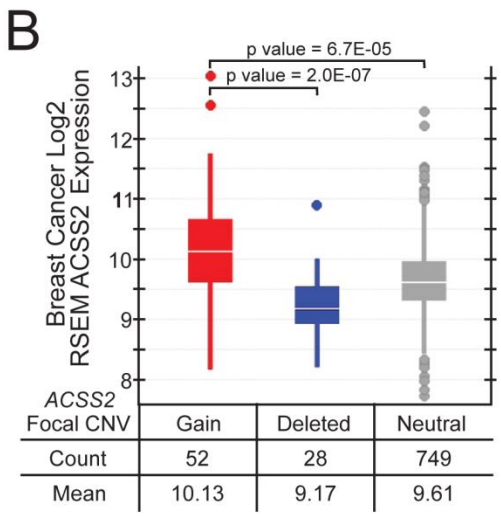

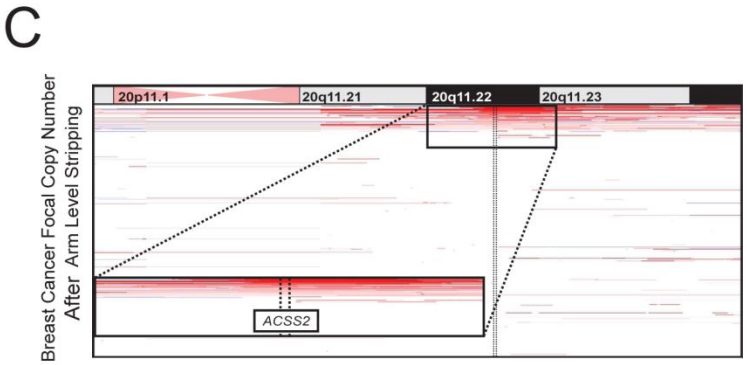

D

Genes on *ACSS2* focal amplicon			
NECAB3	*ITCH*	*MYH7B*	*hsa-mir-1289-1*
C20orf144	*MIR644A*	*MIR499A*	*CEP250*
ACTL10	*hsa-mir-644*	*MIR499B*	*C20orf173*
E2F1	*DYNLRB1*	*hsa-mir-499*	*ERGIC3*
PXMP4	*MAP1LC3A*	*TRPC4AP*	*FER1L4*
ZNF341	*PIGU*	*EDEM2*	*SPAG4*
CHMP4B	*TP53INP2*	*PROCR*	*CPNE1*
RALY	*NCOA6*	*MMP24*	*RBM12*
MIR4755	*HMGB3P1*	*EIF6*	*NFS1*
EIF2S2	*GGT7*	*FAM83C*	*RBM39*
ASIP	***ACSS2***	*UQCC*	*ROMO1*
AHCY	*GSS*	*GDF5*	*PHF20*

Figure S2, related to Figure 2. The ACSS2 Region of Copy Number Gain is Not Associated with Any Other Cancer Consensus Genes. (**A**) OncoPrint of shortlisted targets from the functional screen. Oncoprint was obtained from www.cbioportal.org/public-portal/. Red bars represent copy number gain and upregulation, blue bars represent deletion and downregulation, green bars indicate mutation. Unaltered cases were removed for clarity. (**B**)

ACSS2 exhibited focal gains in DNA copy number in 52/829 breast cancers and was associated with increased ACSS2 expression, with a gain versus deleted raw p = 2.0E-07 and a gain versus neutral arm changes raw p = 6.7E-05 from a student's t test. For boxplots, the white line indicates the median value for each group, boxes represent the 2nd to 3rd quartile, whiskers represent the 1^{rst} to 4^{rth} quartile, and dots represent potential outliers. (**C**) The *ACSS2* amplicon spans across most of genomic region encompassing 20q11.22. (**D**) Genes in the *ACSS2* focal amplicon.

Table S2, related to Figure 2. siRNA Screen Target Gene List and Associated Gene Functions. Provided as an Excel file.

Table S3, related to Figure 2. siRNA Library and Sequences. Provided as an Excel file.

Table S4 related to Figure 2. Strictly Standardized Mean Differences from the siRNA Screens in Hypoxia and Low Serum. Provided as an Excel file.

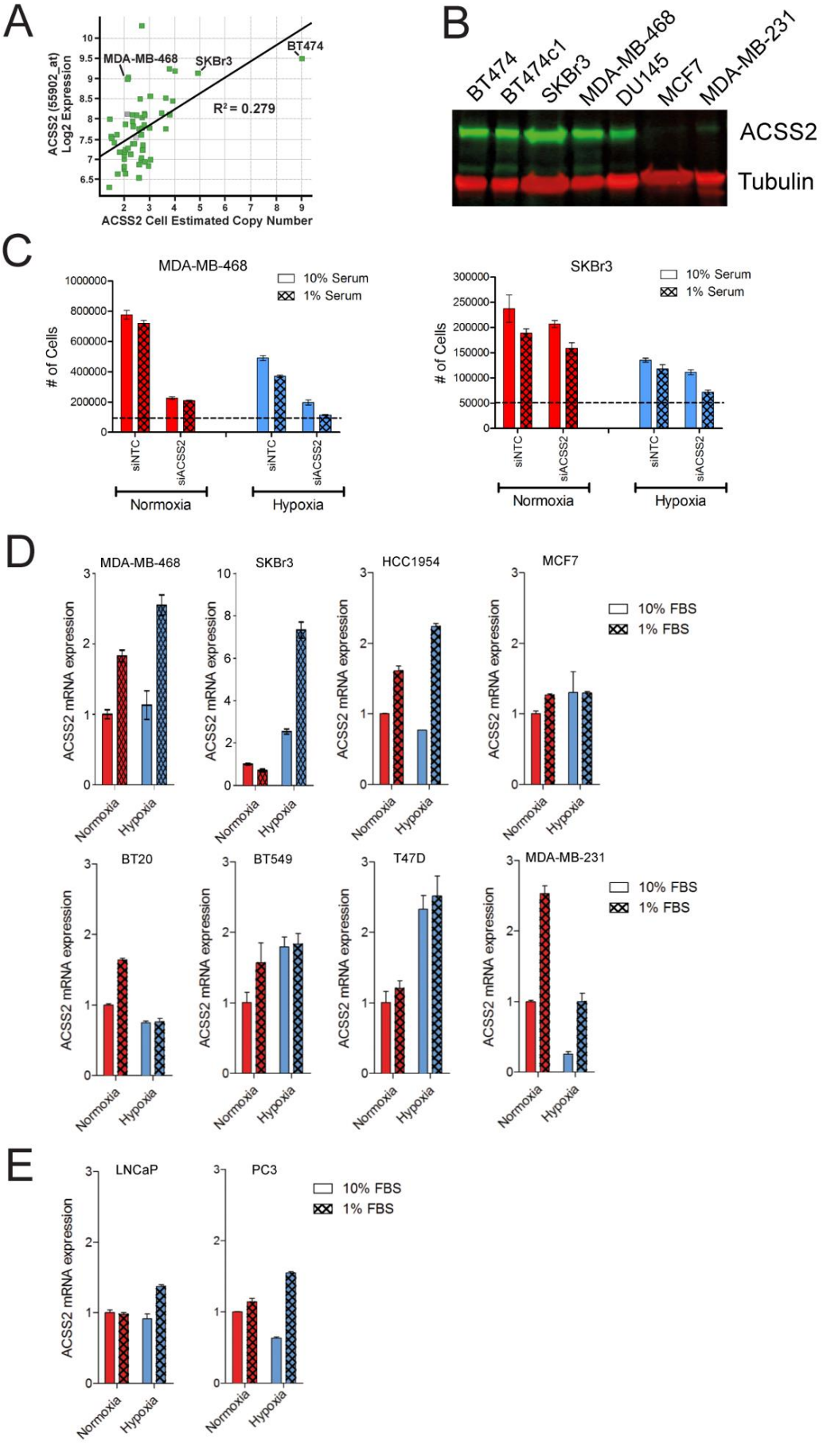
A
ACSS2 (55902_at) Log2 Expression
ACSS2 Cell Estimated Copy Number
MDA-MB-468
SKBr3
BT474
R² = 0.279
B
BT474
BT474c1
SKBr3
MDA-MB-468
DU145
MCF7
MDA-MB-231
ACSS2
Tubulin
C
MDA-MB-468
SKBr3
10% Serum
1% Serum
# of Cells
siNTC
siACSS2
Normoxia
Hypoxia
D
MDA-MB-468
SKBr3
HCC1954
MCF7
BT20
BT549
T47D
MDA-MB-231
ACSS2 mRNA expression
10% FBS
1% FBS
Normoxia
Hypoxia
E
LNCaP
PC3

F

Mutual Exlcusivity (p value)		
Gene	LDHA	PDK1
ACSS2	0.046	0.004
LDHA		<0.001

Tendency towards co-occurrence

G

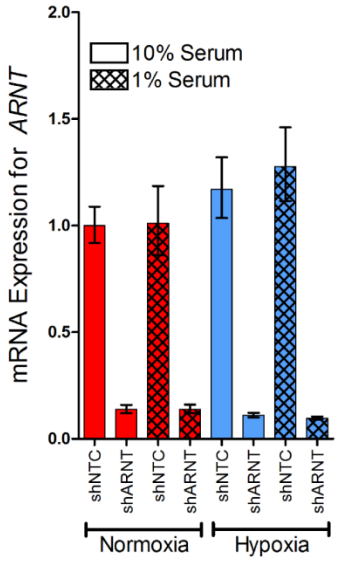

H

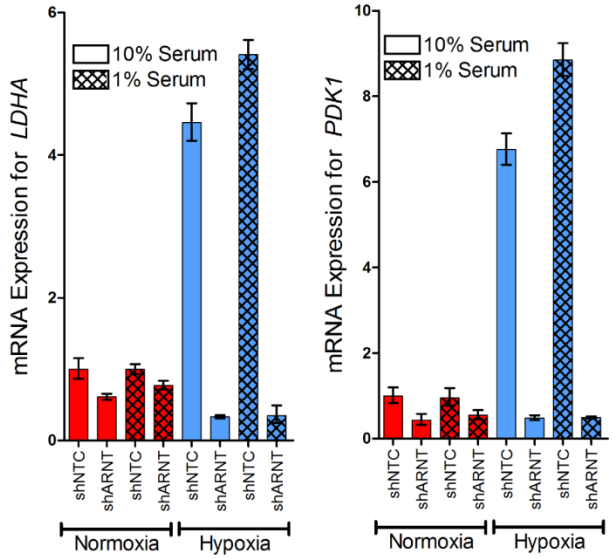

I

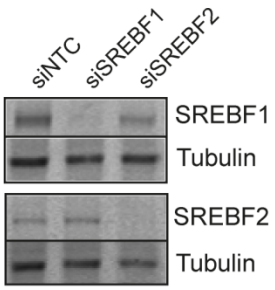

J

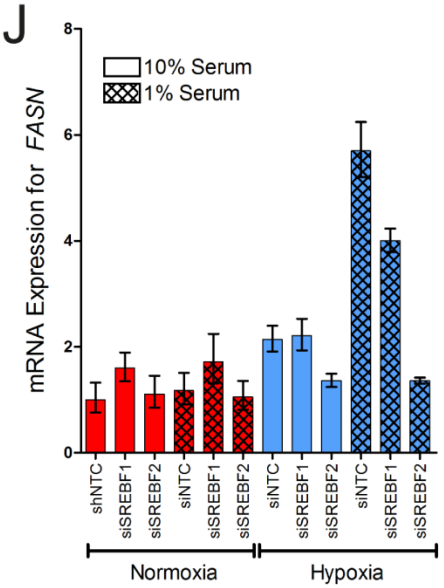

Figure S3, related to Figure 3. Metabolic Stress Upregulates the Expression of ACSS2. (**A**) Plot of ACSS2 mRNA expression versus estimated copy number gain for breast cancer cell lines generated from the Cancer Cell Line Encyclopedia. Affymetrix U133+2 log2 gene expression array data and Affymetrix DNA copy number SNP6.0 array data, converting log2 copy number ratio to estimated copies with the following formula: estimated copy number = (2^(Log2Ratio))*2. Linear regression with an R^2=0.279. (**B**) Immunoblot for ACSS2 in breast and prostate cancer cell lines. (**C**) Growth assay for MDA-MB-468 and SKBr3 cells after siRNA-mediated silencing of ACSS2 during metabolic stress. Dotted lines represent seeding densities. Data are presented as mean ± s.d., (n = 3). (**D**) ACSS2 mRNA expression in breast cancer cell lines under metabolic stress. Error bars represent the mean ± s.e.m. (n = 2). (**E**) ACSS2 mRNA expression in prostate cancer cell lines under metabolic stress. Error bars represent the mean ± s.e.m. (n = 2). (**F**) Co-occurrence of the HIF targets LDHA and PDK1 in a panel of 962 breast cancer patients. Data was obtained from the TCGA database via www.cbioportal.org. $p < 0.05$, Fishers Exact t test. (**G**) Silencing efficiency of the shRNA against ARNT in BT474c1 cells under metabolic stress. Data are presented as mean ± upper and lower limit (n = 3). (**H**) Expression of bona fide HIF targets, LDHA and PDK1 by ARNT silencing in BT474c1 cells under metabolic stress. Data are presented as mean ± upper and lower limit (n = 3). (**I**) Immunoblot of the silencing efficiency of siRNA pools against SREBF1 and SREBF2. (**J**) FASN mRNA expression in BT474c1 cells transfected with a non-targeting control siRNA or a pool of siRNAs against SREBF1 or SREBF2. Data are presented as mean ± upper and lower limit (n = 3).

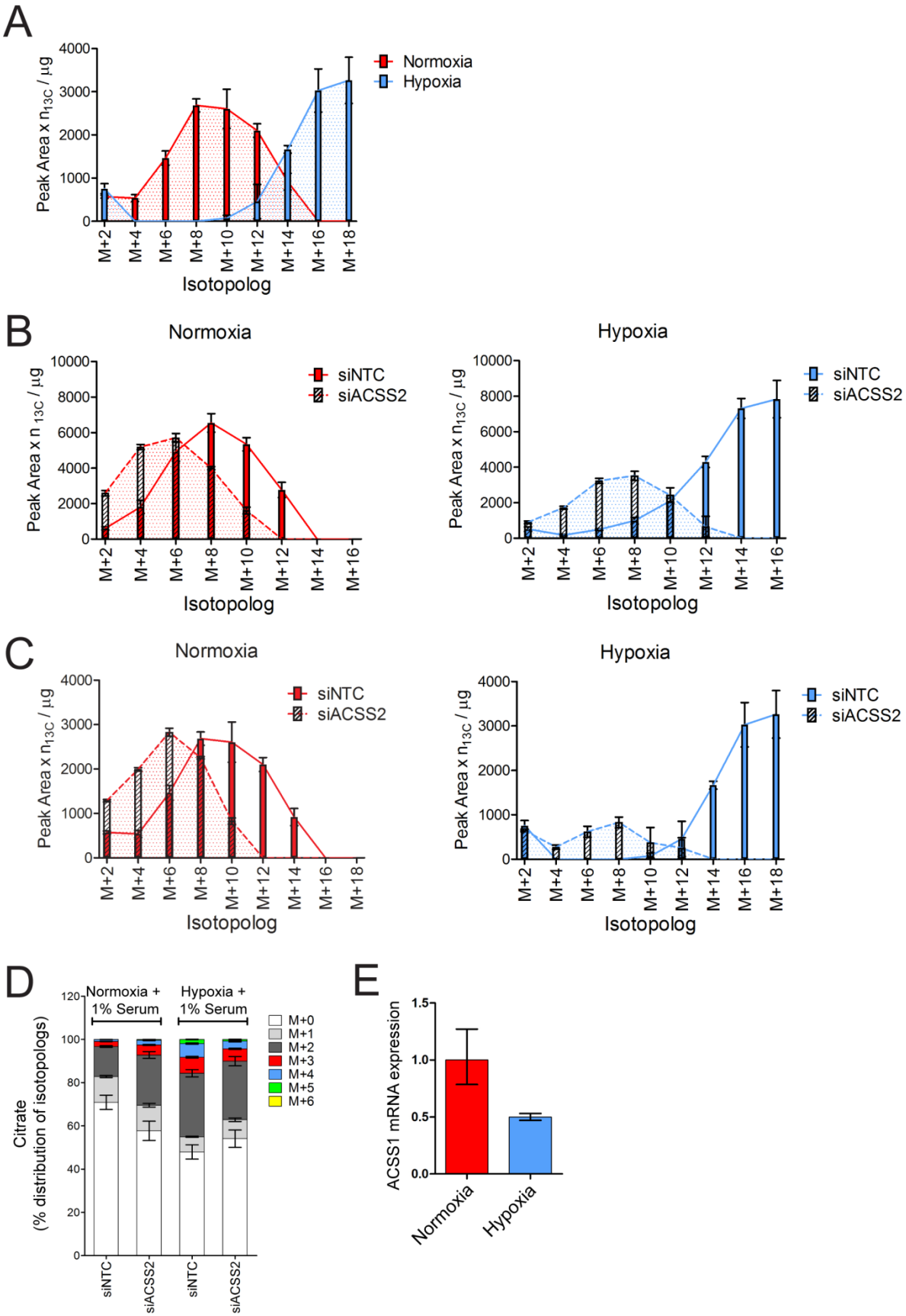
A
Peak Area x n13C / µg
Normoxia
Hypoxia
M+2
M+4
M+6
M+8
M+10
M+12
M+14
M+16
M+18
Isotopolog
B
Normoxia
Hypoxia
siNTC
siACSS2
C
D
Citrate
(% distribution of isotopologs)
Normoxia + 1% Serum
Hypoxia + 1% Serum
M+0
M+1
M+2
M+3
M+4
M+5
M+6
E
ACSS1 mRNA expression

Figure S4, related to Figure 5. ACSS2 Silencing Inhibited Labeling of Palmitate and Stearate by $^{13}C_2$-acetate. (**A**) Isotpolog distribution pattern for stearate in BT474c1 cells cultured in SMEM + 1% serum supplemented with 0.50 mM $^{13}C_2$-acetate. Data are presented as a mean ± s.d. (n = 3) of the weighted contribution of $^{13}C_2$-acetate. The y-axis represents the peak area multiplied by the number (n) of heavy carbon atoms in the isotopolog (i.e. M+2 = 2, M+4 = 4, etc.) (**B**,**C**) Effect of ACSS2 silencing compared to a non-targeting control on the isotpolog distribution pattern for palmitate (B) and stearate (C) in BT474c1 cells cultured in SMEM + 1% serum supplemented with 0.50 mM $^{13}C_2$-acetate. Data are presented as a mean ± s.d. (n = 3) of the weighted contribution of $^{13}C_2$-acetate. (**D**) Data represent the contribution of 0.50 mM $^{13}C_2$-acetate (in SMEM) to citrate synthesis following transfection of the indicated siRNAs into BT474c1 cells. Data are presented as a mean ± s.d. (n = 3). (**E**) ACSS1 expression in BT474c1 cells cultured in SMEM + 1% serum. Data are presented as a mean ± upper and lower limit (n = 3).

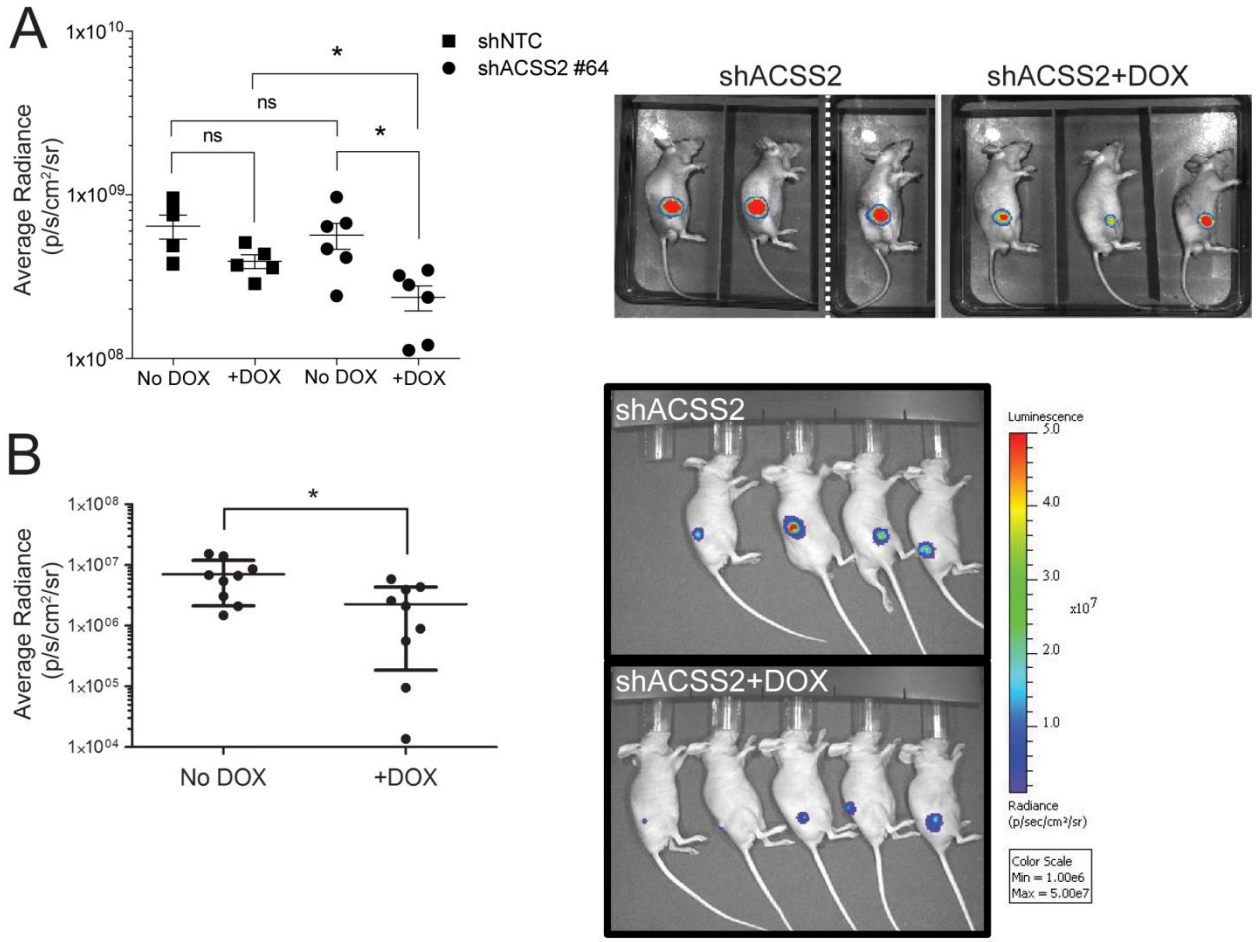
A
shNTC
shACSS2 #64
Average Radiance (p/s/cm²/sr)
1x10^10
1x10^09
1x10^08
ns
ns
*
*
No DOX
+DOX
No DOX
+DOX
shACSS2
shACSS2+DOX
B
Average Radiance (p/s/cm²/sr)
1x10^08
1x10^07
1x10^06
1x10^05
1x10^04
*
No DOX
+DOX
shACSS2
shACSS2+DOX
Luminescence
5.0
4.0
3.0
x10^7
2.0
1.0
Radiance (p/sec/cm²/sr)
Color Scale
Min = 1.00e6
Max = 5.00e7
C
No DOX
+DOX
8-R
6-2R
500 µm
7-L
6-L+R
8-L+R
6-L
D
ACSS2 mRNA expression
2.0
1.5
1.0
0.5
0.0
7-2R
7-R
7-L
7-NM
8-R
8-NM
8-L+R
5-NM
5-L
6-L+R
6-R
6-NM
6-L
6-2R
No Dox
+DOX
No DOX
+DOX

Figure S5, related to Figure 6. Silencing of ACSS2 Expression Inhibited DU145 and MDA-MB-468 Tumor Xenograft Growth. (**A**) Bioluminescence imaging was used to assess the tumor size in DU145 tumor xenografts. Representative images are displayed to the right. Asterisks indicate an unpaired, two-tailed t test, $p < 0.0001$, ns = not significant. Data are presented as mean ± s.d. ($n \geq 5$). (**B**) Bioluminescence imaging was used to assess the tumor size in MDA-MB-468 tumor xenografts. Representative images are displayed to the right. Asterisks indicate an unpaired, two-tailed t test, $p < 0.0001$, Data are presented as mean ± s.d. ($n = 9$) (**C**) Immunohistochemistry for ACSS2 in MDA-MB-468+shACSS2#64 tumors. (**D**) ACSS2 expression in MDA-MB-468+shACSS2#64 tumors. The most right two bars represent the mean ± s.d. ($n = 7$).

SUPPLEMENTAL EXPERIMENTAL PROCEDURES

Generation of Doxycycline-Inducible shRNA Cell Lines

Luciferase was introduced into DU145 and MDA-MD-468 cell lines through retroviral infections using ϕNX-Ampho (ATCC CRL-3213) packaging cells and pBABE-Luciferase. Positive clones were selected in blasticidin S and verified using in vitro luciferase assays (Promega). shRNA sequences targeting ACSS2 or a non-targeting control were cloned into the Tet-pLKO-puro lentiviral vector (Wiederschain et al., 2009). Constructs were validated with sequencing. Lentiviruses were produced by co-transfecting HEK293T cells with lentiviral and packaging plasmids pCMVΔR8.91 and pMD.G (Zufferey et al., 1997). Supernatants containing virus were collected 72 hr after transfection, mixed with polybrene and used to infect cells. Pools were selected in medium containing puromycin. BT474c1 cells were transduced using lentivirus produced from pLKO.1-shNTC, pTRIPZ-Empty, pTRIPZ-shACSS2 vectors (V3THS_366720 and V3THAS_366722; ThermoFisher), or pLKO.1-shARNT by co-transfecting HEK293T cells with packaging plasmids psPAX2 (12260; Addgene) and pCMV-VSV-G (8454; Addgene) (Das et al., 2004). Positive clonal pools were selected in puromycin or additionally sorted on an FACS Aria (BD Biosciences) using tRFP driven off the same promoter.

RNA extraction and qRT-PCR

Total RNA was extracted using an RNeasy kit (Qiagen). 2 μg of RNA was utilized for first strand cDNA synthesis with oligo-dT primers and Superscript II Reverse Transcriptase (Invitrogen). RT-qPCR was performed using SYBR® Green PCR Master Mix (Applied Biosystems) and Quantitect primers (Qiagen) in an ABI PRISM 7900 Sequence Detection System (Applied Biosystems). Relative mRNA expression was calculated using the comparative Ct method after normalization to a loading control. Tumor tissue RNA was extracted as described above and RT-qPCR was performed using the TaqMan gene expression assay for ACSS2 and FASN

(Applied Biosystems). Samples were duplexed with a primer-limited probe for the reference gene (ACTB) and data analyzed as described previously.

siRNA Screen and Data Analysis

Cells were reverse-transfected with 37.5 nM Dharmacon siRNA SMARTpools of 66 genes in 96-well plates using Lullaby reagent (Oz biosciences). After 24 hr, culture medium was replaced with either 10% or 1% FCS containing media and placed in normoxic (20% O_2) or hypoxic conditions (0.1% O_2). 96 hr post-transfection, cells were fixed with 80% ice-cold ethanol, stained with 4′,6-diamidino-2-phenylindole dilactate (DAPI dilactate, Sigma) and cell numbers quantified using an Acumen eX^3 (TPP Labtech) or Operetta (PerkinElmer). Screens were performed in triplicate with positive and negative siRNA controls. The functional screens were replicated at The Beatson Institute and The London Research Institute. Data was analyzed employing the strictly standardized mean difference (Zhang, 2011). Deconvolution was performed using single siRNAs from a separate siRNA pool (Qiagen) and cells were transfected using Lipofectamine RNAiMAX lipofectamine (Invitrogen) according to manufacturer recommendations. Cell number was quantitated using a cell counter (Casy). Pools of siRNAs against SREBF1 or SREBF2 were purchased from Qiagen and transfected using the previously outlined conditions.

Immunohistochemistry, Expression Analysis, and Tissue Studies

Tissue microarray (TMA) slides BR1921a and PR 956 were purchased from US Biomax (Rockville, MD, USA). Tumor sections and TMAs were stained using anti-ACSS2 or pimonidazole as indicated.

Radiolabelled Acetate Uptake and Fatty Acid Synthesis

Cells were seeded onto 2 x 12-well plates 24 hr prior to the experiment in the indicated growth conditions. One plate was transferred to hypoxia the other left in normoxia for a further 24 hr.

The media in each well was changed to SMEM + 10% or 1% serum supplemented with 2 μCi $^{14}C_2$-acetate at 12 hr and 6 hr prior to the end of the experiment. An aliquot of the media was removed from each well and the radioactivity was measured by a scintillation counter and normalized to cell number. A well with no cells and only containing $^{14}C_2$-acetate media only was used as control to normalize uptake. The cells were washed three times in ice cold PBS and then scraped into ice-cold methanol and transferred to silanized glass vial for lipid extraction. Chloroform and 0.88% NaCl were added and the samples were vortexed for 1 min. Samples were centrifuged at 1000 rpm at 4 ^{o}C for 5 min. The lower phase was collected and an equivalent volume from each sample was dried under a nitrogen stream before resuspension in ethanol and counting on the scintillation counter. Data were normalized to cell number.

Quantification of the Immunohistochemistry

Initially the ACSS2 and pimondazole images required registering using landmarks that can be seen in each of the images. Two corresponding points in each image were used to calculate the angle of rotation needed to match the images. Using the image transform function ACSS2 image was rotated by that degree. To overlay the images a landmark point in each image was selected and used to calculate the x,y shift to complete the registration. A mask was generated for regions which stained positive for hypoxia in the pimonidazole image and then split into the individual channels. The red and the green channels were discarded and the blue channel was selected due to the superior contrast of the brown staining. We applied the auto-threshold determined by ImageJ software and smoothed edges and filled holes to reduce noise. We measured the ratio of the amount of ACSS2 staining in hypoxic versus normoxic regions. The ACSS2 image was inverted and an overlay of the hypoxic region mask was applied. The mean grey value per pixel was measured. Likewise, to obtain a value for the normoxic region selection was inverted and again the mean grey value per pixel was measured.

Gas Chromatography and Mass Spectrometry Detection of Acetate

Volumes of 240 μl 100 mM pentafluorobenzyl bromide (PFBBr, Sigma Aldrich) solution in acetone, the derivatizing reagent, were added to medium samples of 120 μl, spiked with $^{13}C_2$ acetate (Cambridge isotopes) as an internal standard. In addition a calibration curve of $^{13}C_2$-acetate of 42-200 μM in medium was used to determine the concentration of ^{12}C-acetate in the media. The solutions were vortexed for 30 sec and incubated for 40 min at 60 ^{o}C. The acetic acid derivatives were extracted by adding 620 μl n-hexane followed by vortexing for 30 sec and centrifugation for 30 sec at 16,100 x g. The organic phase was collected in GC-MS vials and a 2 μl volume was injected with a pulsed split injection mode with a ratio of 10:1 and a 40 psi pressure pulse. The system used was a 7890B gas chromatograph and 7000 triple quad MS, (Agilent) with an Agilent DB-225 (30 m x 250 μm ID x 0.25 μm film) column. The GC was set to an initial temperature of 50 ^{o}C for 2 min, then rising to 220 ^{o}C at 30 ^{o}C/min, with a helium carrier gas flow of 1.5 ml /min. The transfer line was set to 300 ^{o}C and the inlet to 220 ^{o}C. Mass spectra were obtained by positive-ion electron ionization (EI) mode at 70 eV. The acetic acid derivative ions were detected with a MS1 SIM method, scanning for m/z [242] + (^{13}C acetic acid) and m/z [240] + (^{12}C acetic acid) at 8 cycles/sec.

SUPPLEMENTAL REFERENCES

Das, A.T., Zhou, X., Vink, M., Klaver, B., Verhoef, K., Marzio, G., and Berkhout, B. (2004). Viral evolution as a tool to improve the tetracycline-regulated gene expression system. J Biol Chem *279*, 18776-18782.

Wiederschain, D., Wee, S., Chen, L., Loo, A., Yang, G., Huang, A., Chen, Y., Caponigro, G., Yao, Y.M., Lengauer, C.*, et al.* (2009). Single-vector inducible lentiviral RNAi system for oncology target validation. Cell cycle *8*, 498-504.

Zufferey, R., Nagy, D., Mandel, R.J., Naldini, L., and Trono, D. (1997). Multiply attenuated lentiviral vector achieves efficient gene delivery in vivo. Nature biotechnology *15*, 871-875.